JOURNAL OF SPACECRAFT AND ROCKETS
Vol. 40, No. 2, March–April 2003

Aeroelasticity of Composite Aerovehicle Wings in Supersonic Flows

Zhanming Qin,* Liviu Librescu,† and Piergiovanni Marzocca‡
Virginia Polytechnic Institute and State University, Blacksburg, Virginia 24061-0219

A comprehensive aeroelastic model developed toward investigating the static divergence, flutter, and dynamic aeroelastic response of composite aerovehicle wings to sharp-edged gust and blast loads in supersonic flowfield is presented. The aerovehicle wings are modeled as an anisotropic composite thin-walled beam structure featuring circumferentially asymmetric stiffness lay up that generates preferred elastic couplings. A number of nonclassical effects, such as transverse shear, warping restraint, and three-dimensional strain effects, are incorporated in the structural model. Based on the concept of two-dimensional indicial functions considered in conjunction with the aerodynamic strip theory extended to three-dimensional wing model, the unsteady aerodynamic loads in supersonic flows are derived. The effect of elastic tailoring and the implications of transverse shear, warping restraint on divergence and dynamic response of selected wing configurations are investigated, and pertinent conclusions are outlined.

Nomenclature

$Æ$	=	wing aspect ratio, L/b
$a(s)$	=	geometric quantity; see Eq. (2) and Fig. 3
a_{ij}	=	one-dimensional global stiffness coefficients
a_∞	=	undisturbed speed of sound
b, d	=	semichord and semidepth of the beam normal cross section, respectively
b_i	=	inertia coefficient
E_{ij}	=	Young's modulus of orthotropic materials in the material coordinate system
$h(s)$	=	wall thickness as the function of the midline contour s
L	=	wing semispan
$L_{\mathrm{ae}}, T_{\mathrm{ae}}$	=	unsteady aerodynamic lift and moment, respectively
L_b	=	lift caused by the blast
L_g, T_g	=	lift and moment caused by the gust, respectively
l	=	number of the aerodynamic lag terms; see Eqs. (15a) and (15b)
$(M_D)_n$	=	divergence Mach number (chordwise)
M_{Flight}	=	flight Mach number, U_∞/a_∞
$(M_{\mathrm{Flight}})_n$	=	U_n/a_∞
m	=	number of the structural modes included in the actual calculation
m_l	=	number of the constituent layers
$\hat{P}_m$	=	nondimensional pressure intensity, $bP_m/(2b_1U_n^2)$; see Eq. (18)
r	=	pulse length factor of the blast; see Eq. (18)
(s, y, n)	=	local coordinate system; see Fig. 1
t, t_0	=	dimensional time variables
U_∞, U_n	=	streamwise and chordwise freestream speed, respectively, $U_n \equiv U_\infty \cos\Lambda_g$
$u_0(y,t)$, $v_0(y,t)$, $w_0(y,t)$	=	displacement components of the cross section (measured at $x=0$, $z=0$) in x, y, and z directions, respectively
V_G	=	peak gust velocity, a measure of the gust intensity
w_G	=	time-domain gust function
$(\hat{w}_0, \hat{\phi}, \hat{\theta}_x)$	=	nondimensional quantities ($\hat{w}_0 \equiv w_0/2b$, $\hat{\phi} \equiv \phi$, $\hat{\theta}_x \equiv \theta_x$)
$X_{m\times n}$	=	X a $m\times n$ matrix
X^T	=	transpose of the matrix or vector X
(x, y, z)	=	global coordinate system; see Fig. 1
$\gamma_{yz}(y,t)$, $\gamma_{xy}(y,t)$, $\phi(y,t)$	=	transverse shear strains of the cross section and the twist about the y axis, respectively
η	=	nondimensional spanwise coordinate, y/L
$\theta_x(y,t)$, $\theta_z(y,t)$	=	rotations of the cross section about the x, z axes
ϑ	=	ply orientation angle
$/\vartheta_n/$	=	layup scheme
Λ_e	=	effective sweep angle, $\tan\Lambda_e \equiv \tan\Lambda_g/\sqrt{(M_{\mathrm{Flight}}^2-1)}$
Λ_g	=	geometric sweep angle
ρ_∞	=	mass density of the undisturbed flow
τ, τ_0	=	nondimensional time variables, $\tau \equiv U_n t/b$, $\tau_0 \equiv U_n t_0/b$
τ_p	=	positive phase duration of the pressure pulse of the blast; see Eq. (18)
$(\Phi_c)_x$, $(\Phi_{\mathrm{cM}})_x$	=	cross-sectional aerodynamic lift and moment indicial functions to a step change of plunging ($x=0$, the moment about the leading edge; $x=c/2$, about the midchord)
$(\Phi_{\mathrm{cq}})_x$, $(\Phi_{\mathrm{cMq}})_x$	=	cross-sectional aerodynamic lift and moment indicial functions to a step change of pitching ($x=0$, both pitching and the moment about the leading edge; $x=c/2$, about the midchord)
$(\psi_c)_{c/2}$	=	indicial aerodynamic lift caused by the sharp-edged gust
$(\psi_{\mathrm{cM}})_{c/2}$	=	indicial aerodynamic moment (about the midchord) caused by the sharp-edged gust
$\wp(s)$	=	torsional function; see Eq. (4)
$(\dot{()}, \ddot{()})$	≡	$(\partial()/\partial t,\ \partial^2()/\partial^2 t)$
$(\hat{\dot{()}}, \hat{\ddot{()}})$	≡	$(\partial()/\partial\tau,\ \partial^2()/\partial\tau^2)$
$(()', ()'')$	≡	$(\partial()/\partial y,\ \partial^2()/\partial y^2)$
$(\hat{()}', \hat{()}'')$	≡	$(\partial\hat{()}/\partial\eta,\ \partial^2\hat{()}/\partial\eta^2)$

Received 5 March 2002; revision received 19 November 2002; accepted for publication 12 December 2002.

*Research Associate, Department of Engineering Science and Mechanics. Member AIAA.
†Professor, Department of Engineering Science and Mechanics.
‡Postdoctoral Associate, Department of Engineering Science and Mechanics. Member AIAA.

Introduction

BECAUSE of their high structural efficiency and significant potential advantages, thin-walled beam structures made of anisotropic composite materials are likely to be widely used in the design of new generation of flight vehicles. The potential advantages come from the proper exploitation of the material's directionality property, which, in the context of aeroelasticity, has generated a new technology referred to as the aeroelastic tailoring.[1] However, compared with the metallic thin-walled beams, the behavior of the composite ones is much more complex in the sense that it is influenced by a number of important nonclassical effects such as transverse shear, warping inhibition (or warping restraint), nonuniformity of shear stiffness,[2–12] and three-dimensional strain effects.[10,11,13] It is well known that within the classical Euler–Bernoulli beam model the ratio of Young's modulus to transverse shearing modulus is assumed to be zero, implying that the transverse shear stiffness is infinite. However, for anisotropic composite material this ratio can be of the order $\mathcal{O}(100)$. Moreover, for finite span aerovehicle wings featuring nonuniform distribution of the aerodynamic twist moment the classical St. Venant twist model has to be discarded in favor of the restrained twist model. In addition, as revealed in Ref. 5, the nonuniformity of shear stiffness has a significant influence on the warping, and as a result, it has to be considered. Toward a reliable aerovehicle wing design, it is of vital importance to use a structural model that effectively captures these effects and, based on it, to investigate the aeroelastic instability and the aeroelastic response. In fact, during the past two decades, a number of analytical thin-walled beam models have been proposed (e.g., see Refs. 5–7 and 10–15). However, most of the available works have been focused on the modeling and validation (especially static validation),[5,6,12–15] and very few ones have applied the concept of thin-walled beams on the aeroelastic problems (see Refs. 2, 4, 7, and 8 on the static divergence and free-vibration analyses).

A plate-beam model has been used for investigating the warping restraint and transverse shear on the static divergence and flutter instabilities.[16] Because the aerovehicle design is primarily based on the principle of thin-walled beams, it is desirable to investigate the aeroelastic instability and aeroelastic response directly within the framework of thin-walled beams. To the best of the authors' knowledge, the specialized literature devoted to the study of aeroelastic instability and dynamic aeroelastic response of composite aerovehicle wings, which are modeled as anisotropic thin-walled beams in supersonic flows, is quite void of such investigation. In the following section a refined thin-walled beam model that incorporates all of the just-mentioned major nonclassical effects will be adopted. The basic assumptions underlying this model have been proposed in Refs. 4 and 11.

Structural Modeling

A single-cell, closed cross-section, fiber-reinforced composite thin-walled beam is used in the modeling of composite aerovehicle wings toward the study of the dynamic aeroelastic response. As stated in the preceding section, the major nonclassical effects such as transverse shear, anisotropy of the constituent material, warping restraint, and three-dimensional strain effects have to be included in the structural model. In the original formulation of the beam theory,[4,7,8] the variation of contour-wise shear stiffness was not accounted for. However, the theory was later extended to account for these effects in a nonlinear theory.[11] For the geometric configuration and the chosen coordinate system that is usually adopted in the analyses of aerovehicle wings, see Figs. 1–3. Based on the basic assumptions stated in Refs. 4, 7, 8, and 10, the following representation of the three-dimensional displacement quantities is postulated:

$$u(x,y,z,t) = u_0(y,t) + z\phi(y,t) \tag{1a}$$

$$v(x,y,z,t) = v_0(y,t) + \left[x(s) - n\frac{\mathrm{d}z}{\mathrm{d}s}\right]\theta_z(y,t) + \left[z(s) + n\frac{\mathrm{d}x}{\mathrm{d}s}\right]\theta_x(y,t) - [F_w(s) + na(s)]\phi'(y,t) \tag{1b}$$

$$w(x,y,z,t) = w_0(y,t) - x\phi(y,t) \tag{1c}$$

where

$$\theta_x(y,t) = \gamma_{yz}(y,t) - w_0'(y,t)$$
$$\theta_z(y,t) = \gamma_{xy}(y,t) - u_0'(y,t)$$
$$a(s) = -\left(z\frac{\mathrm{d}z}{\mathrm{d}s} + x\frac{\mathrm{d}x}{\mathrm{d}s}\right) \tag{2}$$

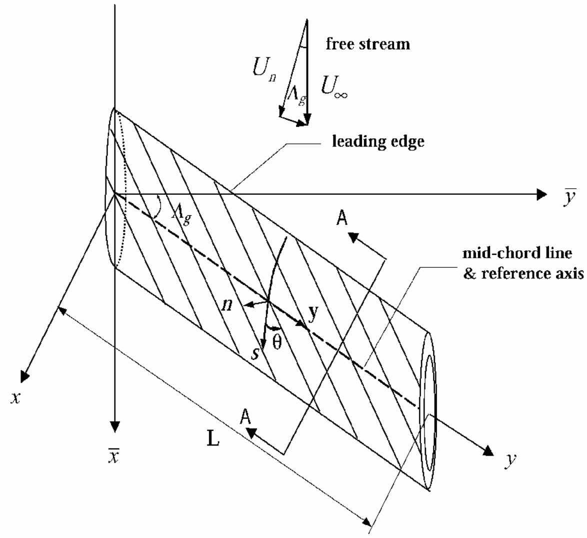

Fig. 1 Geometry of the aerovehicle wing modeled as a thin-walled beam model.

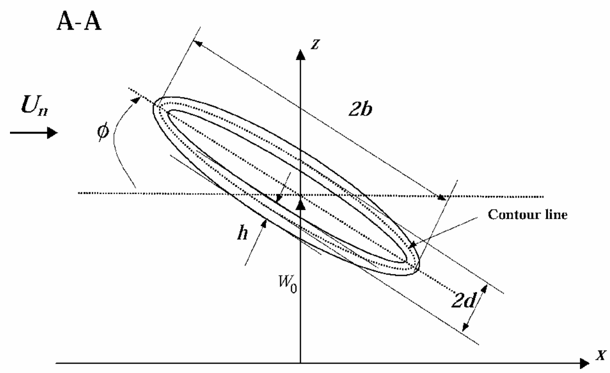

Fig. 2 Geometry of the normal cross section.

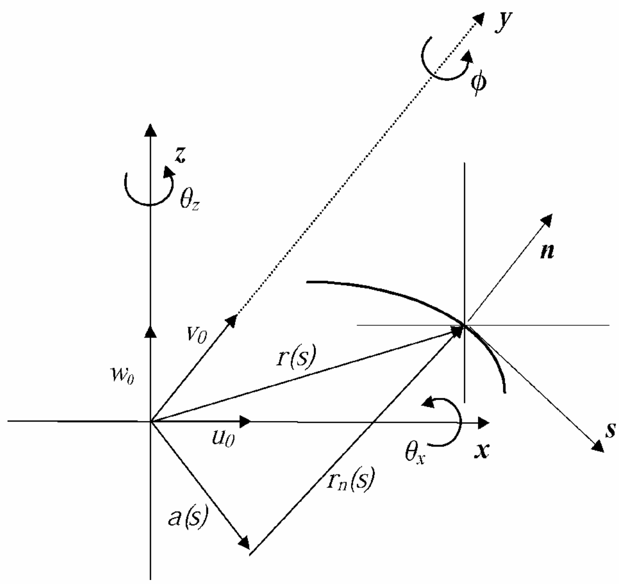

Fig. 3 Displacement field for the beam model: ——, the midline contour.

In the preceding expressions $\theta_x(y,t)$, $\theta_z(y,t)$, and $\phi(y,t)$ denote the rotations of the cross section about the axes x, z and the twist about the y axis, respectively, and $\gamma_{yz}(y,t)$ and $\gamma_{xy}(y,t)$ denote the transverse shear-strain measures.

The warping function in Eq. (1b) is expressed as

$$F_w(s) = \int_0^s [r_n(s) - \wp(s)]\,\mathrm{d}s \tag{3}$$

in which the torsional function $\wp(s)$ and the quantity $r_n(s)$ are expressed as

$$\wp(s) = \frac{\oint_C r_n(\bar{s})\,\mathrm{d}\bar{s}}{h(s)G_{sy}(s)\oint_C[\mathrm{d}\bar{s}/h(\bar{s})G_{sy}(\bar{s})]}$$

$$r_n(s) = z\frac{\mathrm{d}x}{\mathrm{d}s} - x\frac{\mathrm{d}z}{\mathrm{d}s} \tag{4}$$

where $G_{sy}(s)$ is the effective membrane shear stiffness, which is defined as[11]

$$G_{sy}(s) = \frac{N_{sy}}{h(s)\gamma_{sy}^0(s)} \tag{5}$$

N_{sy} denoting membrane shear stress constant.

For the thin-walled beam theory considered here, the six kinematic variables $u_0(y,t), v_0(y,t), w_0(y,t), \theta_x(y,t), \theta_z(y,t), \phi(y,t)$, which represent one-dimensional displacement measures, constitute the basic unknowns of the problem. When the transverse shear effect is ignored, Eq. (2) degenerates to $\theta_x = -w_0'$, $\theta_z = -u_0'$, and as a result, the number of basic unknown quantities reduces to four. Such a case leads to the classical, unshearable beam model.

The strains contributing to the potential energy are as follows.

Spanwise strain:

$$\varepsilon_{yy}(n,s,y,t) = \varepsilon_{yy}^0(s,y,t) + n\varepsilon_{yy}^n(s,y,t) \tag{6a}$$

where

$$\varepsilon_{yy}^0(s,y,t) = v_0'(y,t) + \theta_z'(y,t)x(y,t) - \phi''(y,t)F_w(s) \tag{6b}$$

$$\varepsilon_{yy}^n(s,y,t) = -\theta_z'(y,t)\frac{\mathrm{d}z}{\mathrm{d}s} + \theta_x'(y,t)\frac{\mathrm{d}x}{\mathrm{d}s} - a(s)\phi''(y,t) \tag{6c}$$

are the axial strain components associated with the primary and secondary warping, respectively.

Tangential shear strain:

$$\gamma_{sy}(s,y,t) = \gamma_{sy}^0(s,y,t) + \wp(s)\phi'(y,t) \tag{7a}$$

where

$$\gamma_{sy}^0(s,y,t) = \gamma_{xy}\frac{\mathrm{d}x}{\mathrm{d}s} + \gamma_{yz}\frac{\mathrm{d}z}{\mathrm{d}s} = (u_0' + \theta_z)\frac{\mathrm{d}x}{\mathrm{d}s} + (w_0' + \theta_x)\frac{\mathrm{d}z}{\mathrm{d}s} \tag{7b}$$

Transverse shear-strain measure:

$$\gamma_{\mathrm{ny}}(s,y,t) = -\gamma_{xy}\frac{\mathrm{d}z}{\mathrm{d}s} + \gamma_{yz}\frac{\mathrm{d}x}{\mathrm{d}s} = -(u_0' + \theta_z)\frac{\mathrm{d}z}{\mathrm{d}s} + (w_0' + \theta_x)\frac{\mathrm{d}x}{\mathrm{d}s} \tag{8}$$

The stress resultants and stress couples can be reduced to the following expressions:

$$\begin{Bmatrix} N_{yy} \\ N_{sy} \\ L_{yy} \\ L_{sy} \end{Bmatrix} = \begin{bmatrix} K_{11} & K_{12} & K_{13} & K_{14} \\ K_{21} & K_{22} & K_{23} & K_{24} \\ K_{41} & K_{42} & K_{43} & K_{44} \\ K_{51} & K_{52} & K_{53} & K_{54} \end{bmatrix} \begin{Bmatrix} \varepsilon_{yy}^0 \\ \gamma_{sy}^0 \\ \phi' \\ \varepsilon_{yy}^n \end{Bmatrix} \tag{9a}$$

$$N_{\mathrm{ny}} = \left(A_{44} - A_{45}^2/A_{55}\right)\gamma_{\mathrm{ny}} \tag{9b}$$

in which the reduced stiffness coefficients K_{ij}, the stress resultants N_{yy}, N_{sy}, and the stress couples L_{yy}, L_{sy} are defined in Appendix A. As to the systematic validation of the preceding structural model, the reader is referred to Ref. 17.

Time-Domain Aerodynamic Loads in Supersonic Flows: An Indicial Function Approach

Unsteady Aerodynamic Loads

Compared with the mature and deeply entrenched oscillatory compressible unsteady aerodynamic models, the indicial function-based aerodynamic models (see Ref. 18, pp. 367–375) provide an efficient approach for describing the compressible unsteady flow. The efficiency stems from the facts that 1) once the proper indicial functions are available, the linearized unsteady aerodynamic loads to arbitrary small motion can be derived through Duhamel's convolution; 2) the indicial functions involved can be derived/approximated via various approaches, such as rational approximation, formulation by computational fluid dynamics (CFD)[19]; or with the aid of experiments[20]; 3) derivation of indicial functions via CFD can be several orders faster than the direct CFD simulations.[19] In fact, based on the concept of indicial functions a unified representation of linear unsteady aerodynamic loads in incompressible, compressible subsonic and supersonic flows can be developed. In case of two-dimensional incompressible flow the indicial function is the classical Wagner function; extensions of the concept of indicial functions to two- or three-dimensional unsteady compressible subsonic and supersonic flows were conducted by numerous investigators (see Refs. 18–22 and the references therein). By the Volterra integral theory this concept has been extended to nonlinear aerodynamics (see Refs. 23 and 24) and applied to the modeling of gust-induced aerodynamic loads (see Ref. 18, pp. 286–288 and 374).

In this section, in conjunction with the aerodynamic strip theory, a set of analytical two-dimensional indicial functions in supersonic flow derived in exact form (see Ref. 18, pp. 371 and 372) are adopted toward the study of dynamic aeroelastic response of three-dimensional aerovehicle wings. For the investigation of aeroelastic instability of composite structures, additional advantage emerging from their use consists of the possibility of simultaneously investigating both the static and dynamic aeroelastic instabilities.[25] An extensive validation of two-dimensional indicial functions in selected flight speed regimes, such as the incompressible, subsonic compressible, supersonic, and high supersonic ones, is provided in Ref. 21.

The vertical velocity of fluid particles forced by the wing motion (positive upward) can be expressed in nondimensional form as

$$w_a(\hat{x},\eta,\tau) = U_n\left[\left(2\dot{\hat{w}}_0 - \hat{\phi} + \frac{2}{\mathit{AR}}\frac{\partial\hat{w}_0}{\partial\eta}\tan\Lambda_e\right) - \hat{x}\left(\dot{\hat{\phi}} + \frac{1}{\mathit{AR}}\frac{\partial\hat{\phi}}{\partial\eta}\tan\Lambda_e\right)\right] \triangleq U_n(\hat{w}_{\mathrm{aT}} - \hat{x}\dot{\hat{\phi}}_{\mathrm{aP}}) \tag{10a}$$

where we define

$$\hat{w}_{\mathrm{aT}}(\eta,\tau) \equiv \left(2\dot{\hat{w}}_0 - \hat{\phi} + \frac{2}{\mathit{AR}}\frac{\partial\hat{w}_0}{\partial\eta}\tan\Lambda_e\right)$$

$$\dot{\hat{\phi}}_{\mathrm{aP}}(\eta,\tau) \equiv \left(\dot{\hat{\phi}} + \frac{1}{\mathit{AR}}\frac{\partial\hat{\phi}}{\partial\eta}\tan\Lambda_e\right) \tag{10b}$$

Denote $(\Phi_c)_0(\tau)$, $(\Phi_{\mathrm{cM}})_0(\tau)$ as the indicial lift and moment functions (about the leading edge, as denoted by the subscript 0) caused by the unit step change of the vertical translational velocity. The subscript c represents "compressible." As a result, the aerodynamic lift and moment about the midchord (taken as the reference axis; see Fig. 1) are

$$L_T(\eta,\tau) = -\pi\rho_\infty U_n^2(2b)\left\{[\hat{w}_{\mathrm{aT}}(\eta,0) + \dot{\hat{\phi}}_{\mathrm{aP}}(\eta,0)](\Phi_c)_0(\tau) + \int_0^\tau \frac{\partial[\hat{w}_{\mathrm{aT}}(\eta,\sigma) + \dot{\hat{\phi}}_{\mathrm{aP}}(\eta,\sigma)]}{\partial\sigma}(\Phi_c)_0(\tau-\sigma)\,\mathrm{d}\sigma\right\} \tag{11a}$$

$$T_{\mathrm{yT}}(\eta,\tau) = -\pi\rho_\infty U_n^2(2b)^2\left\{[\hat{w}_{\mathrm{aT}}(\eta,0)+\dot{\hat{\phi}}_{\mathrm{aP}}(\eta,0)](\Phi_{\mathrm{cM}})_0(\tau) + \int_0^\tau \frac{\partial[\hat{w}_{\mathrm{aT}}(\eta,\sigma)+\dot{\hat{\phi}}_{\mathrm{aP}}(\eta,\sigma)]}{\partial\sigma}(\Phi_{\mathrm{cM}})_0(\tau-\sigma)\,\mathrm{d}\sigma\right\} + bL_T(\eta,\tau) \tag{11b}$$

where the ratio $(\Phi_{\mathrm{cM}})_0(\tau)/(\Phi_c)_0(\tau)$ measures the location of the aerodynamic center (fraction of the whole chord length from the leading edge). Upon denoting $(\Phi_{\mathrm{cq}})_0(\tau)$, $(\Phi_{\mathrm{cMq}})_0(\tau)$ as the indicial lift and moment functions (about the leading edge) as a result of the unit step change of the pitching rate at the leading edge, the corresponding aerodynamic lift and moment about the midchord are

$$L_q(\eta,\tau) = 2\pi\rho_\infty U_n^2(2b)\left\{[\dot{\hat{\phi}}_{\mathrm{aP}}(\eta,0)](\Phi_{\mathrm{cq}})_0(\tau) + \int_0^\tau \frac{\partial\dot{\hat{\phi}}_{\mathrm{aP}}(\eta,\sigma)}{\partial\sigma}(\Phi_{\mathrm{cq}})_0(\tau-\sigma)\,\mathrm{d}\sigma\right\} \tag{12a}$$

$$T_{\mathrm{yq}}(\eta,\tau) = 2\pi\rho_\infty U_n^2(2b)^2\left[\dot{\hat{\phi}}_{\mathrm{aP}}(\eta,0)(\Phi_{\mathrm{cMq}})_0(\tau) + \int_0^\tau \frac{\partial\dot{\hat{\phi}}_{\mathrm{aP}}(\eta,\sigma)}{\partial\sigma}(\Phi_{\mathrm{cMq}})_0(\tau-\sigma)\,\mathrm{d}\sigma\right] + bL_q(\eta,\tau) \tag{12b}$$

Similarly, the ratio $(\Phi_{\mathrm{cMq}})_0(\tau)/(\Phi_{\mathrm{cq}})_0(\tau)$ measures the location of the aerodynamic center (fraction of the whole chord length from the leading edge). The coefficient 2π in Eqs. (11) and (12) is not related to the incompressible lift slope. Instead, the influence of compressibility is embedded entirely in the indicial functions $(\Phi_c)_0(\tau)$, $(\Phi_{\mathrm{cq}})_0(\tau)$, $(\Phi_{\mathrm{cM}})_0(\tau)$, and $(\Phi_{\mathrm{cMq}})_0(\tau)$ (see Ref. 18, pp. 367–375).

As a result, the total unsteady aerodynamic lift L_{ae} (positive upwards) and the moment about the midchord T_{ae} (positive nose up) are

$$\begin{aligned} L_{\mathrm{ae}}(\eta,\tau) &= L_T(\eta,\tau) + L_q(\eta,\tau) \\ &= -\pi\rho_\infty U_n^2(2b)\left[\hat{w}_{\mathrm{aT}}(\eta,0)(\Phi_c)_{c/2}(\tau) + \int_0^\tau \frac{\partial\hat{w}_{\mathrm{aT}}(\eta,\sigma)}{\partial\sigma}(\Phi_c)_{c/2}(\tau-\sigma)\,\mathrm{d}\sigma\right] \\ &\quad + 2\pi\rho_\infty U_n^2(2b)\left[\dot{\hat{\phi}}_{\mathrm{aP}}(\eta,0)(\Phi_{\mathrm{cq}})_{c/2}(\tau) + \int_0^\tau \frac{\partial\dot{\hat{\phi}}_{\mathrm{aP}}(\eta,\sigma)}{\partial\sigma}(\Phi_{\mathrm{cq}})_{c/2}(\tau-\sigma)\,\mathrm{d}\sigma\right] \end{aligned} \tag{13a}$$

$$\begin{aligned} T_{\mathrm{ae}}(\eta,\tau) &= T_{\mathrm{yT}}(\eta,\tau) + T_{\mathrm{yq}}(\eta,\tau) \\ &= -\pi\rho_\infty U_n^2(2b)^2\left[\hat{w}_{\mathrm{aT}}(\eta,0)(\Phi_{\mathrm{cM}})_{c/2}(\tau) + \int_0^\tau \frac{\partial\hat{w}_{\mathrm{aT}}(\eta,\sigma)}{\partial\sigma}(\Phi_{\mathrm{cM}})_{c/2}(\tau-\sigma)\,\mathrm{d}\sigma\right] \\ &\quad + 2\pi\rho_\infty U_n^2(2b)\left[\dot{\hat{\phi}}_{\mathrm{aP}}(\eta,0)(\Phi_{\mathrm{cMq}})_{c/2}(\tau) + \int_0^\tau \frac{\partial\dot{\hat{\phi}}_{\mathrm{aP}}(\eta,\sigma)}{\partial\sigma}(\Phi_{\mathrm{cMq}})_{c/2}(\tau)\,\mathrm{d}\sigma\right] \end{aligned} \tag{13b}$$

where

$$(\Phi_c)_{c/2}(\tau) = (\Phi_c)_0(\tau)$$

$$(\Phi_{\mathrm{cMq}})_{c/2}(\tau) = (\Phi_{\mathrm{cMq}})_0(\tau) - \tfrac{1}{2}(\Phi_{\mathrm{cM}})_0(\tau) + \tfrac{1}{2}(\Phi_{\mathrm{cq}})_0(\tau) - \tfrac{1}{4}(\Phi_c)_0(\tau) \tag{14a}$$

$$(\Phi_{\mathrm{cM}})_{c/2}(\tau) = (\Phi_{\mathrm{cM}})_0(\tau) + \tfrac{1}{2}(\Phi_c)_0(\tau)$$

$$(\Phi_{\mathrm{cq}})_{c/2}(\tau) = (\Phi_{\mathrm{cq}})_0(\tau) - \tfrac{1}{2}(\Phi_c)_0(\tau) \tag{14b}$$

To facilitate the solution of the aeroelastic system, the preceding indicial functions are approximated by quasi-polynomials:

$$(\Phi_c)_{c/2}(\tau) = A_0^c + \sum_{i=1}^{l} A_i^c \exp\left(-\beta_i^c\tau\right)$$

$$(\Phi_{\mathrm{cM}})_{c/2}(\tau) = A_0^{\mathrm{cM}} + \sum_{i=1}^{l} A_i^{\mathrm{cM}} \exp\left(-\beta_i^{\mathrm{cM}}\tau\right) \tag{15a}$$

$$(\Phi_{\mathrm{cq}})_{c/2}(\tau) = A_0^{\mathrm{cq}} + \sum_{i=1}^{l} A_i^{\mathrm{cq}} \exp\left(-\beta_i^{\mathrm{cq}}\tau\right)$$

$$(\Phi_{\mathrm{cMq}})_{c/2}(\tau) = A_0^{\mathrm{cMq}} + \sum_{i=1}^{l} A_i^{\mathrm{cMq}} \exp\left(-\beta_i^{\mathrm{cMq}}\tau\right) \tag{15b}$$

in which β_i^c, β_i^{cq}, β_i^{cM}, and β_i^{cMq} are two-dimensional unsteady aerodynamic lag coefficients.

In this paper three aerodynamic lag terms are used for each indicial function, that is, totally 12 aerodynamic lag terms are needed to describe the two-dimensional unsteady aerodynamic loads in the supersonic flowfield. Note that the preceding indicial functions are dependent on the flight Mach number. The implementation of the approximation is based on the nonlinear curve fitting functions provided by Mathematica™. The comparison of the approximation against the exact Lomax's indicial functions[18] are displayed in Fig. 4.

Aerodynamic Loads Caused by Sharp-Edged Gust and Blast in Supersonic-Flows

The discrete sharp-edged gust model used herein can be expressed as

$$w_G(\tau) = H(\tau)V_G \tag{16}$$

where V_G is a measure of gust intensity and $H(\tau)$ is the unit step function. In this paper it is assumed that the gust intensity is uniformly distributed along the wing span. Based on the Duhamel's integral and the indicial functions $(\psi_c)_{c/2}(\tau)$ and $(\psi_{\mathrm{cM}})_{c/2}(\tau)$ for the supersonic entry into the sharp-edged gust, the two-dimensional lift $L_g(\tau)$ and moment $T_g(\tau)$ per unit span can be expressed as

$$L_g(\tau) = 2\pi\rho_\infty bU_n^2\int_0^\tau \frac{w_G(\tau_0)}{U_n}\frac{\partial(\psi_c)_{c/2}(\tau-\tau_0)}{\partial\tau}\,\mathrm{d}\tau_0 \tag{17a}$$

$$T_g(\tau) = 2\pi\rho_\infty(2b^2)U_n^2\int_0^\tau \frac{w_G(\tau_0)}{U_n}\frac{\partial(\psi_{\mathrm{cM}})_{c/2}(\tau-\tau_0)}{\partial\tau}\,\mathrm{d}\tau_0 \tag{17b}$$

The two-dimensional supersonic indicial functions $(\psi_c)_{c/2}(\tau)$ and $(\psi_{\mathrm{cM}})_{c/2}(\tau)$ used in this paper are provided in Ref. 18, p. 374.

The blast load from a sonic-boom signature can be modeled as an N-shaped pressure pulse[26,27]:

$$L_b(\tau) = P_m(1-\tau/\tau_p)[H(\tau) - H(\tau - r\tau_p)] \tag{18}$$

in which P_m is the peak reflected pressure in excess to the ambient pressure, τ_p is the positive phase duration of the pressure pulse, and r is the pulse length factor.[26,27] When $r = 1$, the N-shaped pulse degenerates into an explosive pulse (in triangular form), and when $r = 2$, a symmetric sonic-boom pulse is obtained.[26] For the blast loads we assume that these are uniformly distributed throughout the wing, implying that no aerodynamic torsional moment is induced as a result of the blast in terms of the reference axis.

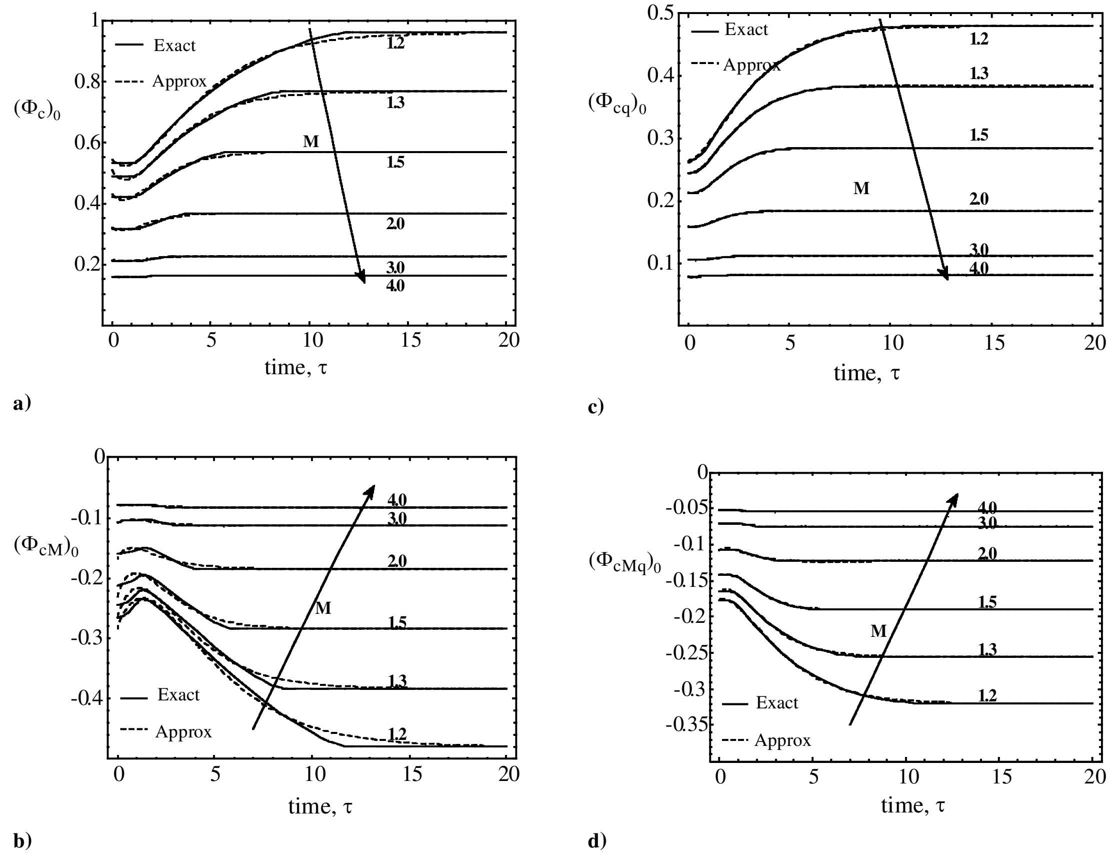

Fig. 4 Nonlinear curve fitting of the unsteady two-dimensional (airfoil) aerodynamic indicial functions. (Exact indicial functions are from Ref. 18. *M* is the flight Mach number.)

Aeroelastic Governing Equations and Solution Methodology

Aeroelastic Governing Equations and Boundary Conditions

The aeroelastic governing equations and the boundary conditions can be systematically derived from the extended Hamilton's Principle,[28] which states that the true path of motion renders the following variational form stationary:

$$\int_{t_1}^{t_2} (\delta\mathcal{T} - \delta\mathcal{V} + \overline{\delta W_e})\,\mathrm{d}t = 0 \tag{19a}$$

with

$$\delta u_0 = \delta v_0 = \delta w_0 = \delta\theta_x = \delta\theta_z = \delta\phi = 0 \quad \text{at } t = t_1 \text{ and } t_2 \tag{19b}$$

where δ is the variational operator, $\mathcal{T}$ and $\mathcal{V}$ denote the kinetic energy and strain energy, respectively, and $\overline{\delta W_e}$ denotes the virtual work caused by external forces. For the problem at hand, these terms are defined as follows.

Kinetic energy:

$$\mathcal{T} = \frac{1}{2}\int_0^L \oint_C \sum_{k=1}^{m_l} \int_{h_{(k)}} \rho_{(k)} \left[\left(\frac{\partial u}{\partial t}\right)^2 + \left(\frac{\partial w}{\partial t}\right)^2 + \left(\frac{\partial v}{\partial t}\right)^2\right] \mathrm{d}n\,\mathrm{d}s\,\mathrm{d}y \tag{20}$$

Strain energy:

$$V = \frac{1}{2}\int_\tau \sigma_{ij}\varepsilon_{ij}\,\mathrm{d}\tau = \frac{1}{2}\int_0^L \oint_C \sum_{k=1}^{m_l} \int_{h_{(k)}} [\sigma_{yy}\varepsilon_{yy} + \sigma_{sy}\gamma_{sy} + \sigma_{\mathrm{ny}}\gamma_{\mathrm{ny}}]_{h_{(k)}}\,\mathrm{d}n\,\mathrm{d}s\,\mathrm{d}y \tag{21}$$

Virtual work caused by unsteady aerodynamic and gust loads:

$$\overline{\delta W_e} = \int_0^L [p_z(y,t)\delta w_0(y,t) + m_y(y,t)\delta\phi(y,t)]\,\mathrm{d}y \tag{22}$$

In Eq. (22) the total lift per unit span is $p_z(y,t) = L_{\mathrm{ae}} + L_g + L_b$, and total twist moment per unit span is $m_y(y,t) = T_{\mathrm{ae}} + T_g$. The conjugate pairs $(\sigma_{\mathrm{ss}}, \varepsilon_{\mathrm{ss}})$ and $(\sigma_{\mathrm{sn}}, \gamma_{\mathrm{sn}})$ do not contribute to the total strain energy $\mathcal{V}$ (based on assumptions 1 and 5; see Ref. 17) and hence do not appear in Eq. (21). To study the aeroelastic problems featuring bending-twist elastic coupling, a beam configured by circumferentially asymmetric stiffness (CAS) lay up[5,8] and characterized by a biconvex cross section is considered. As demonstrated in Refs. 7, 8, and 29, this type of beam features two independent sets of elastic couplings: 1) elastic coupling among vertical bending/twist/vertical transverse shear and 2) elastic coupling among extension/lateral bending/lateral transverse shear. Moreover, the aerodynamic loads and the inertia forces of this type of beam automatically split into the preceding two groups; hence, the equations of motion and the boundary conditions are completely decoupled. Therefore, for the problem at hand the second group in the just-mentioned sets can be safely discarded.

In terms of the basic unknowns, the governing equations that account for warping inhibition and transverse shear are[30]

$$\delta w_0\text{:}\; a_{55}(w_0'' + \theta_x') + \underline{\underline{a_{56}\phi'''}} + L_{\mathrm{ae}} + L_g + L_b - b_1\ddot{w}_0 = 0 \tag{23a}$$

$$\delta\phi\text{:}\; a_{37}\theta_x'' + a_{77}\phi'' - a_{56}(w_0''' + \theta_x'') - \underline{\underline{a_{66}\phi^{(IV)}}} + T_{\mathrm{ae}} + T_g - (b_4 + b_5)\ddot{\phi} + \underline{\underline{(b_{10} + b_{18})\ddot{\phi}''}} = 0 \tag{23b}$$

$$\delta\theta_x\text{:}\; a_{33}\theta_x'' + a_{37}\phi'' - a_{55}(w_0' + \theta_x) - \underline{\underline{a_{56}\phi''}} - \underline{(b_4 + b_{14})\ddot{\theta}_x} = 0 \tag{23c}$$

Boundary conditions:
At $y = 0$,

$$w_0 = 0, \qquad \phi = 0, \qquad \underline{\underline{\phi' = 0}}, \qquad \theta_x = 0 \tag{24a}$$

At $y = L$,

$$\delta w_0\text{: } a_{55}(w_0' + \theta_x) + \underline{\underline{a_{56}\phi''}} = 0$$

$$\delta\phi\text{: } -a_{56}(w_0'' + \theta_x') - \underline{\underline{a_{66}\phi'''}} + a_{37}\theta_x' + a_{77}\phi' = -(b_{10} + b_{18})\ddot{\phi}'$$

$$\underline{\underline{\delta\phi'}}\text{: } -a_{56}(w_0' + \theta_x) - \underline{\underline{a_{66}\phi''}} = 0$$

$$\delta\theta_x\text{: } a_{33}\theta_x' + a_{37}\phi' = 0 \tag{24b}$$

In the preceding equations the terms underscored by double solid lines are associated with the warping inhibition effect, whereas the term underscored by a single solid line identifies the rotatory inertia effect.[4,7–9] Inertia coefficients b_1, b_4, b_5, b_{10}, b_{18}, b_{14} and the one-dimensional beam stiffness a_{ij} are defined in Appendix A. For the unshearable beam model (i.e., infinitely rigid in transverse shear strains) the substitution of $a_{55}(w_0' + \theta_x)$ obtained from Eq. (23c) into Eq. (23a) and in the first natural boundary condition in Eqs. (24b), followed by the replacement of θ_x by $-w_0'$, results in the pertinent governing equations:

$$\delta w_0: -a_{33}w_0^{(IV)} + a_{37}\phi''' + L_{\text{ae}} + L_g$$

$$+ L_b - b_1\ddot{w}_0 + (b_4 + b_{14})\ddot{w}_0'' = 0 \tag{25a}$$

$$\delta\phi: -a_{37}w_0''' + a_{77}\phi'' - a_{66}\phi^{(IV)} + T_{\text{ae}}$$

$$+ T_g - (b_4 + b_5)\ddot{\phi} + (b_{10} + b_{18})\ddot{\phi}'' = 0 \tag{25b}$$

and the boundary conditions:

At $y = 0$,

$$w_0 = 0, \qquad w_0' = 0, \qquad \phi = 0, \qquad \phi' = 0 \tag{26a}$$

At $y = L$,

$$\delta w_0: a_{33}w_0''' - a_{37}\phi'' - (b_4 + b_{14})\ddot{w}_0' = 0$$

$$\delta w_0': -a_{33}w_0'' + a_{37}\phi' = 0$$

$$\delta\phi: a_{66}\phi''' + a_{37}w_0'' - a_{77}\phi' - (b_{10} + b_{18})\ddot{\phi}' = 0$$

$$\delta\phi': a_{66}\phi'' = 0 \tag{26b}$$

State-Space Solution

Because of the complicated boundary conditions and the elastic couplings involved in the differential governing equations, the Extended Galerkin's Method (EGM)[31,32] is used to discretize the associated boundary-value/eigenvalue problems. The underlying idea of this method is to select weight functions that need only fulfill the geometric boundary conditions (see Appendix B for the details of shape functions used). As a result, the natural boundary conditions that might not be fulfilled appear as a residual in the functional, which should be minimized in the Galerkin's sense.[31] After semidiscretization by EGM, we cast the approximated solution of the aeroelastic system into the following nondimensional state-space form:

$$\begin{Bmatrix} \dot{\hat{\boldsymbol{x}}}_s \\ \dot{\hat{\boldsymbol{x}}}_a \end{Bmatrix} = \begin{bmatrix} \boldsymbol{A}_s & \boldsymbol{B}_s \\ \boldsymbol{B}_a\boldsymbol{A}_s & \boldsymbol{A}_a + \boldsymbol{B}_a\boldsymbol{B}_s \end{bmatrix} \begin{Bmatrix} \hat{\boldsymbol{x}}_s \\ \hat{\boldsymbol{x}}_a \end{Bmatrix} + \begin{bmatrix} \boldsymbol{0}_{m\times 1} \\ \bar{\boldsymbol{M}}_n^{-1} \\ \boldsymbol{D}_2\bar{\boldsymbol{M}}_n^{-1} \\ \vdots \\ \boldsymbol{D}_2\bar{\boldsymbol{M}}_n^{-1} \end{bmatrix} \{\boldsymbol{Q}_g + \boldsymbol{Q}_b\} \tag{27}$$

or in a more compact form, as

$$\{\dot{\hat{\boldsymbol{X}}}\} = [\boldsymbol{A}]\{\hat{\boldsymbol{X}}\} + [\boldsymbol{B}_e]\{\boldsymbol{Q}_g + \boldsymbol{Q}_b\} \tag{28}$$

Herein, $\hat{\boldsymbol{x}}_s$ and $\hat{\boldsymbol{x}}_a$ are $2m \times 1$, $lm \times 1$ vectors, which describe the motion of the wing and unsteady aerodynamic loads on the wing, respectively. $\boldsymbol{Q}_g$ is the generalized gust and $\boldsymbol{Q}_b$ the generalized blast loads. The details of the matrices and vectors in Eqs. (27) and (28) are listed in Appendix B.

Discarding the term associated with the gust and blast loads from Eq. (28) (i.e., the last term on the right-hand side), we obtain the solution of aeroelastic instabilities (e.g., static divergence, flutter).

Analysis of Static and Dynamic Aeroelastic Instabilities

The divergence and flutter instability solutions can be derived systematically from Eq. (28) by discarding the gust and blast loads $\boldsymbol{Q}_g(\tau)$ and $\boldsymbol{Q}_b(\tau)$. For the static divergence of restrained wings (i.e., wings for which the rigid-body motion is discarded), the unsteady aerodynamic terms involving time derivatives become immaterial, which leads to the equation

$$\left(k_r\bar{\boldsymbol{K}}_s + \frac{1}{8\mu_0}\frac{1}{\sqrt{(M_{\text{Flight}})_n^2 - 1}}\bar{\bar{\boldsymbol{K}}}_{\text{ae}}\right)\hat{\boldsymbol{q}} = \boldsymbol{0} \tag{29}$$

where the matrix $\bar{\bar{\boldsymbol{K}}}_{\text{ae}}$ and the coefficient k_r are defined in Appendix B.

The static divergence corresponds to the minimum flight speed that renders Eq. (29) to have a nontrivial solution, which leads to

$$\det\left[k_r\bar{\boldsymbol{K}}_s + \frac{1}{8\mu_0}\frac{1}{\sqrt{(M_{\text{Flight}})_n^2 - 1}}\bar{\bar{\boldsymbol{K}}}_{\text{ae}}\right] = 0 \tag{30}$$

The flutter corresponds to an eigenvalue problem. Let $\hat{\boldsymbol{x}} = \bar{\hat{\boldsymbol{x}}}e^{\lambda\tau}$, from Eq. (28) and discarding the external loads, we get

$$(\lambda\boldsymbol{I} - \boldsymbol{A})\bar{\hat{x}} = \boldsymbol{0} \tag{31}$$

From the linear system stability theory, when all of the eigenvalues of $\boldsymbol{A}$ are within the left half Laplace plane, that is, when $\forall Re[\lambda^*(\boldsymbol{A})] < 0$, the system is stable, where $\lambda^*(\boldsymbol{A})$ denotes an eigenvalue of $\boldsymbol{A}$. When there exists $Re[\lambda^*(\boldsymbol{A})] > 0$, the system is unstable. The flutter solution corresponds to the minimum critical flight speed that renders the system to transit from stable motion to unstable motion. At this transition state

$$Re[\lambda^*(\boldsymbol{A})] = 0 \tag{32}$$

Here $\boldsymbol{A}$ is the system matrix in Eq. (31). The imaginary part of that eigenvalue corresponds to the flutter frequency.

Solution of the Dynamic Aeroelastic Response

The general solution of Eq. (28) can be expressed as[28]

$$\{\hat{\boldsymbol{X}}(\tau)\} = [e^{A\tau}]\{\hat{\boldsymbol{X}}(0)\} + \int_0^\tau \left[e^{A(\tau-\tau_0)}\right][\boldsymbol{B}_e]\{\boldsymbol{Q}_g(\tau_0) + \boldsymbol{Q}_b(\tau_0)\}\,\mathrm{d}\tau_0 \tag{33}$$

where the transition matrix

$$[e^{A\tau}] = \mathcal{L}^{-1}[(p\boldsymbol{I} - \boldsymbol{A})^{-1}] = \sum_{i=0}^{\infty}\left(\frac{\boldsymbol{A}^i}{i!}\right)\tau^i$$

For a general nonconservative system its eigenvalues and eigenvectors are complex valued quantities. Although the system matrix $\boldsymbol{A}$ can be orthogonalized in terms of its left and right eigenvectors,[28] for large order of $\boldsymbol{A}$ the actual implementation of the modal analysis is not efficient.[28] Moreover, the Laplace transform method is almost impractical for systems featuring large orders. Therefore, the preceding equation is directly discretized in the time domain. With the fixed sampling step $\Delta\tau$ the following discretized equation is derived[28]:

$$\{\hat{\boldsymbol{X}}(k+1)\} = [e^{A\Delta\tau}]\{\hat{\boldsymbol{X}}(k)\} + [\boldsymbol{A}]^{-1}[e^{A\Delta\tau} - \boldsymbol{I}][\boldsymbol{B}_e]\{\boldsymbol{Q}_g(k) + \boldsymbol{Q}_b(k)\} \tag{34}$$

where the discretized transition matrix is defined as

$$[e^{A\Delta\tau}] = \sum_{i=0}^{\infty}\frac{\boldsymbol{A}^i}{i!}(\Delta\tau)^i \tag{35}$$

Table 1 Comparison of the calculated flutter results of Goland's wing

Method	Description	Flutter speed (Mach no.)	Flutter frequency, Hz
Exact	Two-dimensional incompressible flow	$M_{\mathrm{Flutter}} = 0.40$	$f_{\mathrm{Flutter}} = 11.25$
EGM[a]	$N = 7$, two-dimensional incompressible flow, transient method[b]	$M_{\mathrm{Flutter}} = 0.40$	$f_{\mathrm{Flutter}} = 11.15$
EGM	$N = 7$, two-dimensional compressible flow, transient method[c]	$M_{\mathrm{Flutter}} = 0.38$	$f_{\mathrm{Flutter}} = 10.90$

[a]Extended Galerkin's method.
[b]Jones's approximation of Wagner's function is used.[18]
[c]Leishman's indicial functions are used.[20]

Given the maximum amplitude of the eigenvalues of $\boldsymbol{A}$ and the sampling step $\Delta\tau$, the numerical convergence requirement of the preceding equation and the prescribed computational accuracy determine the number of truncated terms in Eq. (35) for the approximation of $[e^{A\Delta\tau}]$ (Ref. 28). In this paper the accuracy order of 10^{-5} is prescribed. Once the solution of $\hat{\boldsymbol{X}}(k)$ is known, the generalized coordinate $\hat{\xi}_s(k)$ can be extracted, and then the aeroelastic response (e.g., shearable model) can be reconstructed as follows:

$$\hat{w}_0(\eta, k) = \hat{\boldsymbol{\Psi}}_w^T(\eta)\hat{\boldsymbol{\Theta}}_w\hat{\xi}_s(k), \qquad \hat{\phi}(\eta, k) = \hat{\boldsymbol{\Psi}}_\phi^T(\eta)\hat{\boldsymbol{\Theta}}_\phi\hat{\xi}_s(k)$$

$$\hat{\theta}_x(\eta, k) = \hat{\boldsymbol{\Psi}}_x^T(\eta)\hat{\boldsymbol{\Theta}}_x\hat{\xi}_s(k) \tag{36}$$

where $\hat{\boldsymbol{\Psi}}_w(\eta)$, $\hat{\boldsymbol{\Psi}}_\phi(\eta)$, and $\hat{\boldsymbol{\Psi}}_x(\eta)$ are $N \times 1$ shape function vectors and $\boldsymbol{\Theta}_w$, $\boldsymbol{\Theta}_\phi$, $\boldsymbol{\Theta}_x$ are $N \times m$ eigenvectors (see Appendix B).

Validation

The aeroelastic model based on the representation of unsteady aerodynamic loads by indicial functions can be applied to the cases of incompressible, subsonic compressible, and supersonic flows. For the purpose of validation, as a first step, the flutter predictions of Goland's wing[33] in incompressible and subsonic compressible flows are calculated by using the transient method. The predictions are then compared against the available result in the literature[33] (Table 1). In the preceding transient method, Jones's quasi-polynomial approximation of Wagner's function is used. It is readily seen that the correlation is excellent and the offset of flutter speed and flutter frequency by the transient method is well within the approximation accuracy of Wagner's function. It is also observed that the compressibility only causes about 5.0% decrease of the flutter speed and 2.2% decrease of the flutter frequency compared with the predictions by the incompressible model. This is consistent with the well-known fact that at the lower range of the compressible subsonic speeds the effect of compressibility on flutter is quite small. As for the validation in case of supersonic flight speed, the rectangular wing specified in Ref. 34 is used. Further specifications of this wing are $b = 1.0$ m, $GJ = 6.0 \times 10^6 \mathrm{N \cdot m^2}$, and the air density is taken at the sea level ($\rho_\infty = 1.225$ kg/m^3). The prediction by the present model using the same shape functions as in Ref. 34 is $(M_{\mathrm{Flutter}})_n = 1.33$, whereas the flutter prediction extracted from Fig. 12 in Ref. 34 is $(M_{\mathrm{Flutter}})_n = 1.26$ (by using the two-dimensional aerodynamic coefficients). The critical supersonic flutter speed predicted by the present model is obtained by starting from high flight speed and gradually reducing the flight speed until the critical point is encountered. This qualitative characteristics can be readily verified by Fig. 12 in Ref. 34.

Numerical Results and Discussion

In this section the static divergence and dynamic aeroelastic response of anisotropic thin-walled beams exposed to selected gust and blast loads are investigated. The influence of ply orientation, sweep angle, aspect ratio, and the implication of warping restraint as well as transverse shear effects on divergence and the response are also investigated. Depending on the design objectives and model/tools to be used, there are many other design parameters contributing to the broad range effects of the aeroelastic tailoring.[1] The geometric specifications of the beams with CAS lay-up configuration are listed in Table 2. The material properties of the test thin-walled beams are listed here: $E_{11} = 206.8 \times 10^9$ N/m^2, $E_{22} = E_{33} = 5.17 \times 10^9$ N/m^2, $G_{13} = G_{23} = 2.55 \times 10^9$ N/m^2, $G_{12} = 3.10 \times 10^9$ N/m^2, $\mu_{12} = \mu_{13} = \mu_{23} = 0.25$, and $\rho = 1.528 \times 10^3$ Kg/m^3. In the actual calculation the first five structural modes and three aerodynamic lag terms for each indicial function [see Eqs. (15a–15d)] are used, that is, $m = 5$, $l = 3$, all of the response components (bending, twist, and transverse) are measured at the beam tip ($\eta = 1$), and the gust intensity is specified as $V_G = 15$ m/s for the test cases. Sea-level air density ($\rho_\infty = 1.225$ kg/m^3) is used in all of the following cases.

Table 2 Geometric specifications of the test wings

Parameter	Value
Width $2b^a$, m	0.757
Depth $2d^a$, m	0.0997
Wall thickness h, m	0.0203
Number of layers	6
Layer thickness, m	0.0034
Layup scheme of the walls	$/\vartheta_6/$

[a]Length is measured on the midline contour.

Table 3 Influence of ply angle and sweep angle on the static divergence

Ply angle, deg	$(M_D)_n$		
	$\Lambda_g = -15$ deg	$\Lambda_g = -30$ deg	$\Lambda_g = -45$ deg
90	78.80	36.56	21.09
105	No divergence	No divergence	No divergence
120	No divergence	No divergence	6.76
135	No divergence	4.10	N/A[a]
150	5.55	N/A	N/A
165	2.37	N/A	N/A
180	1.59	N/A	N/A

[a]Value is below the supersonic flight speed range.

Table 4 Effect of warping restraint and transverse shear on the static divergence ($\Lambda_g = 0$ deg)

$\mathcal{R}$	$(M_D)_n$		
	WR + TS	WR + NTS[a]	FW + TS[b]
		$\vartheta = 45$ deg	
5	5.291	5.294 (0.06%[c])	4.691 (−12.8%)
6	2.877	2.877 (0.0%)	2.558 (−12.5%)
7	N/A[d]	N/A	N/A
		$\vartheta = 75$ deg	
5	10.001	10.153 (1.51%)	7.601 (−31.6%)
6	5.473	5.535 (1.12%)	4.316 (−26.8%)
7	3.230	3.261 (0.92%)	2.575 (−25.4%)

[a]Warping restraint model, transverse shear discarded.
[b]Free-warping model, transverse shear incorporated.
[c]Percentage in the second column is in terms of the unshearable model (i.e., WR + NTS), and in the third column is in terms of the free-warping model (i.e., FW + TS).
[d]Value is below the supersonic flight speed range.

Table 3 displays the influence of ply angle and geometric sweep angle on divergence speed of a composite aerovehicle wing. The related parameter is $\mathcal{R} = 6$. It is readily seen that changing ply orientation has a dramatic influence on the static divergence speed. For example, even for the swept-forward wing with $\Lambda_g = -45$ deg the static divergence can still be effectively controlled by arranging ply angle within the range of [90, 120] deg.

Table 4 shows the influence of warping restraint and transverse shear on the divergence speed of wings of different aspect ratios. Warping restraint has a significant influence on the divergence speed. However, compared with the warping restraint effect, on the selected wing, transverse shear has a much smaller influence on the divergence speed.

Figures 5–7 display the response of a wing featuring various ply angles and exposed to a sharp-edged gust. It can be seen that the

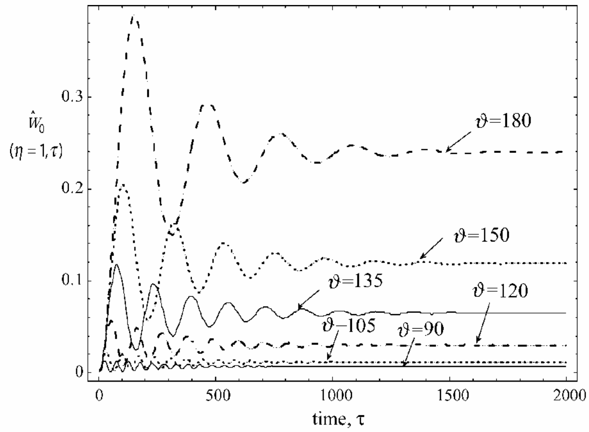

Fig. 5 Influence of ply angle on the deflection response to a sharp-edged gust [ϑ: deg; other parameters: $(M_{\text{Flight}})_n = 2.5$, $\text{AR} = 6$, $\Lambda_g = 0$ deg].

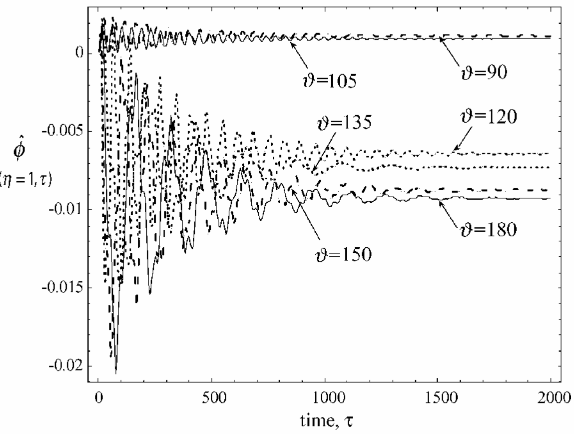

Fig. 6 Influence of ply angle on the twist response to a sharp-edged gust [ϑ: deg; other parameters: $(M_{\text{Flight}})_n = 2.5$, $\text{AR} = 6$, $\Lambda_g = 0$ deg].

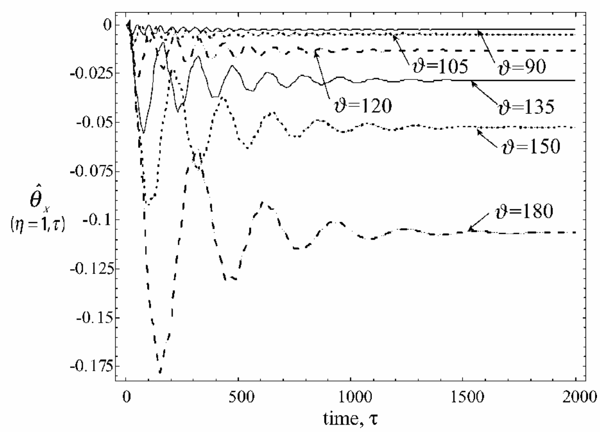

Fig. 7 Influence of ply angle on the response of $\hat{\theta}_x(\eta = 1, \tau)$ to a sharp-edged gust [ϑ: deg; other parameters: $(M_{\text{Flight}})_n = 2.5$, $\text{AR} = 6$, $\Lambda_g = 0$ deg].

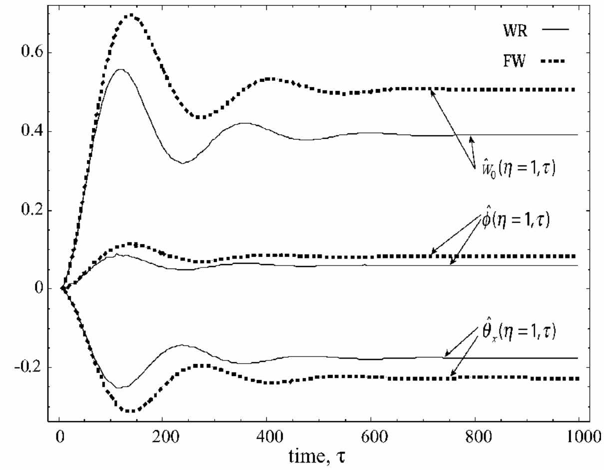

Fig. 8 Warping restraint effect on the response of a wing to a sharp-edged gust [$(M_{\text{Flight}})_n = 1.5$, $/45_6/$, $\text{AR} = 6$, $\Lambda_g = 0$ deg].

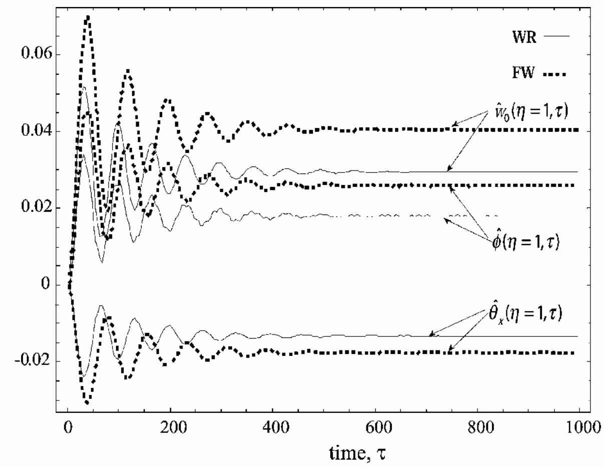

Fig. 9 Warping restraint effect on the response of a wing to a sharp-edged gust [$(M_{\text{Flight}})_n = 1.5$, $/75_6/$, $\text{AR} = 6$, $\Lambda_g = 0$ deg].

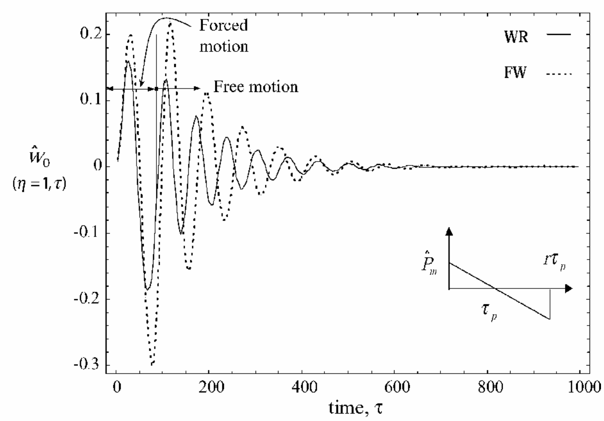

Fig. 10 Warping restraint effect on the response of a wing to a sonic boom [$(M_{\text{Flight}})_n = 1.5$, $/45_6/$, $\text{AR} = 6$, $\Lambda_g = 0$ deg, $\hat{P}_m = 10^{-3}$, $r = 2$, $\tau_p = 40$; sonic-boom pulse is included in the inset].

directionality property of composite materials used here plays a dramatic influence on the response amplitudes related to bending, twist, and transverse shear. No structural damping is considered, and the damping is entirely of aerodynamic nature.

Figures 8 and 9 display the influence of warping restraint on the response of a wing exposed to a sharp-edged gust, and Fig. 10 displays the influence of warping restraint on the response of the wing exposed to a sonic boom. The corresponding parameters are shown within these figures. It is shown that subjected to the sharp-edged gust the amplitude of the steady response predicted by the warping restraint model can be 25% less than that predicted by the free-warping counterpart. However, considering warping restraint effect does not always lead to the overall stiffening results, as shown by Fig. 11. The overall destiffening phenomenon is caused by the interaction between warping restraint stiffening effect and the elastic coupling. Specifically, free-warping assumption tends to decrease the twist stiffness. However, the influence of elastic coupling on the twist stiffness in the case of $/135_6/$ layup outweighs this decrease. Interestingly enough, for the static aeroelastic response a similar phenomenon was reported when a plate-beam wing model was used in Ref. 35.

Table 5 Influence of flight speed on the steady-state response to a sharp-edged gust

$(M_{\text{Flight}})_n$	$\hat{w}_0(\eta=1, \tau\to\infty)$	$\hat{\phi}(\eta=1, \tau\to\infty)$	$\hat{\theta}_x(\eta=1, \tau\to\infty)$
1.5	0.391	0.060	−0.176
2.0	0.464	0.071	−0.207
2.5	1.09	0.168	−0.491
2.6	1.458	0.225	−0.656
2.8	12.073	1.886	−5.515
2.88	Divergence	Divergence	Divergence
3.0	Divergence	Divergence	Divergence

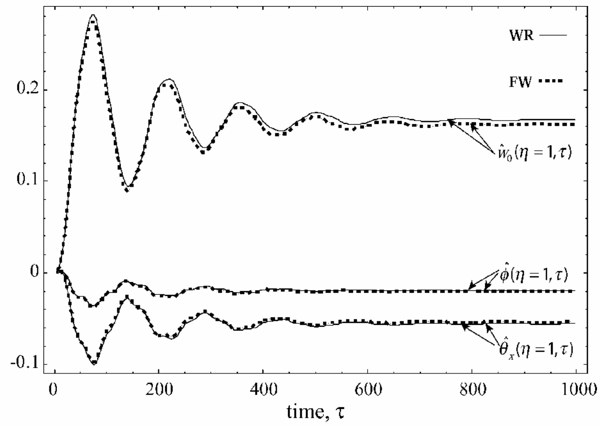

Fig. 11 Warping restraint effect on the response of a wing to a sharp-edged gust [$(M_{\text{Flight}})_n = 1.5$, /135$_6$/, AR = 6, $\Lambda_g = 0$ deg].

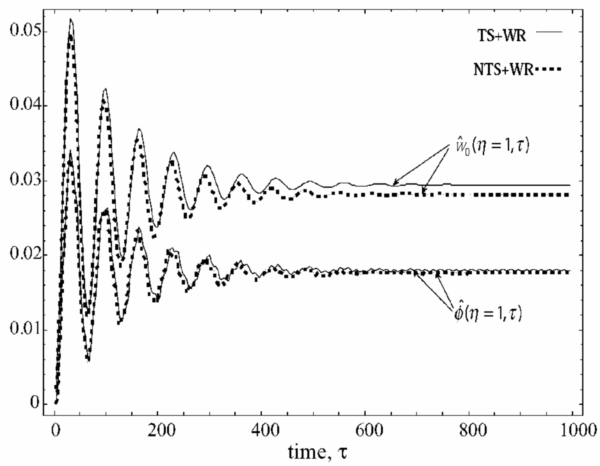

Fig. 12 Transverse shear effect on the response of a wing to a sharp-edged gust [$(M_{\text{Flight}})_n = 1.5$, /75$_6$/, AR = 6, $\Lambda_g = 0$ deg].

Figures 12 and 13 display the influence of transverse shear on the response of a wing exposed to a sharp-edged gust and to a sonic boom, respectively. Compared with the warping restraint effect, the effect of transverse shear on the response of the selected wing is much weaker.

Table 5 shows the influence of flight speed on the steady-state response to a sharp-edged gust. The related parameters are /45$_6$/, AR $= 6$, $\Lambda_g = 0$ deg. Between the flight Mach numbers 2.8 and 2.88, there exists a divergence instability onset for the selected wing. Directly using the divergence instability analysis, we get the divergence speed $(M_D)_n = 2.877$ (see Table 4). Because static divergence and flutter instabilities are simultaneously addressed in this model, it is concluded that for the selected wing configuration (AR $= 6$, /45$_6$/, $\Lambda_g = 0$ deg), the static divergence speed is lower than the flutter speed. This phenomenon is consistent with a trend reported in Ref. 36, which shows that for some specific wings and in the backward fiber sweep quadrant, that is, ϑ in [0, 90] deg, the divergence instability is more critical than flutter instability. Figure 14 displays the time history of the response to a sharp-edged gust for various flight Mach numbers. When $(M_D)_n = 3.0$, the wing is already in the state of aeroelastic divergence instability.

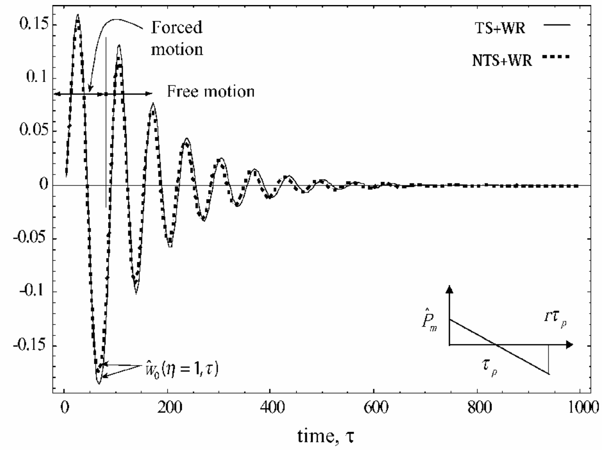

Fig. 13 Transverse shear effect on the response of a wing to a sonic boom [$(M_{\text{Flight}})_n = 1.5$, /75$_6$/, AR = 6, $\Lambda_g = 0$ deg, $\hat{P}_m = 10^{-3}$, $r = 2$, $\tau_p = 40$; sonic-boom pulse is included in the inset].

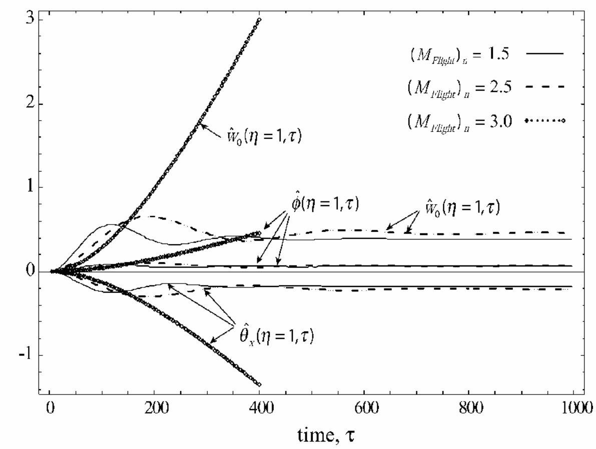

Fig. 14 Dynamic aeroelastic response of a wing to a sharp-edged gust for different flight speeds (/45$_6$/, AR = 6, $\Lambda_g = 0$ deg).

Conclusions

The problems of static divergence, flutter, and dynamic aeroelastic response of composite aerovehicle wings modeled as anisotropic thin-walled beams in a supersonic flowfield and exposed to selected gust and blast loads have been approached in a unified way. Based on this well-encompassing aeroelastic model developed here, the implications of ply orientation, sweep angle, aspect ratio, warping restraint, and transverse shear on the divergence and dynamic aeroelastic response are specifically investigated. It is shown that the directionality properties featured by advanced composite materials can play a significant role toward the passive control of both static divergence and dynamic aeroelastic response of aerovehicle wings. Warping restraint has a significant influence on both the divergence and dynamic response on the selected wing configurations, and the trend illustrated in the numerical simulations reveals that the lower the aspect ratio, the more prominent its influence becomes. As a result, warping restraint effect has always to be included when addressing the aeroelastic behavior of supersonic aerovehicles. Compared with the warping restraint effect on the static divergence and response, the influence of transverse shear appears to be much weaker. The validation reveals a good agreement of the predictions between the current model and those from the specialized available literature.

The present study can be used for predesign and optimization of such type of aerovehicle wings in supersonic flowfield.

Appendix A: Expressions of One-Dimensional Stiffness and Mass Terms

Listed next are the global stiffness quantities $a_{ij} (= a_{ji})$ related to the problem addressed in this paper:

$$a_{33} = \oint_C \left[z^2 K_{11} + 2z \frac{\mathrm{d}x}{\mathrm{d}s} K_{14} + \left(\frac{\mathrm{d}x}{\mathrm{d}s} \right)^2 K_{44} \right] \mathrm{d}s$$

$$a_{37} = \oint_C \left[z K_{13} + \frac{\mathrm{d}x}{\mathrm{d}s} K_{43} \right] \mathrm{d}s$$

$$a_{55} = \oint_C \left[\left(\frac{\mathrm{d}z}{\mathrm{d}s} \right)^2 K_{22} + \left(\frac{\mathrm{d}x}{\mathrm{d}s} \right)^2 \bar{A}_{44} \right] \mathrm{d}s$$

$$a_{56} = -\oint_C \left[F_w \frac{\mathrm{d}z}{\mathrm{d}s} K_{21} + a(s) \frac{\mathrm{d}z}{\mathrm{d}s} K_{24} \right] \mathrm{d}s$$

$$a_{66} = \oint_C \left[F_w^2 K_{11} + 2F_w a(s) K_{14} + a(s)^2 K_{44} \right] \mathrm{d}s$$

$$a_{77} = \oint_C \wp(s) K_{23} \, \mathrm{d}s$$

where $\bar{A}_{44} = A_{44} - A_{45}^2/A_{55}$; K_{ij} are the reduced stiffness coefficient defined as

$$K_{11} = A_{22} - \frac{A_{12}^2}{A_{11}}, \qquad K_{12} = A_{26} - \frac{A_{12}A_{16}}{A_{11}} = K_{21}$$

$$K_{13} = \left(A_{26} - \frac{A_{12}A_{16}}{A_{11}} \right) \wp(s), \qquad K_{14} = B_{22} - \frac{A_{12}B_{12}}{A_{11}} = K_{41}$$

$$K_{22} = A_{66} - \frac{A_{16}^2}{A_{11}}, \qquad K_{23} = \left(A_{66} - \frac{A_{16}^2}{A_{11}} \right) \wp(s)$$

$$K_{24} = B_{26} - \frac{A_{16}B_{12}}{A_{11}} = K_{42}, \qquad K_{43} = \left(B_{26} - \frac{B_{12}A_{16}}{A_{11}} \right) \wp(s)$$

$$K_{44} = D_{22} - \frac{B_{12}^2}{A_{11}}, \qquad K_{51} = B_{26} - \frac{B_{16}A_{12}}{A_{11}}$$

$$K_{52} = B_{66} - \frac{B_{16}A_{16}}{A_{11}}, \qquad K_{53} = \left(B_{66} - \frac{B_{16}A_{16}}{A_{11}} \right) \wp(s)$$

$$K_{54} = D_{26} - \frac{B_{12}B_{16}}{A_{11}}$$

The inertia coefficients in Eqs. (23–26) are defined as

$$b_1 = \oint_C m_0 \, \mathrm{d}s, \qquad (b_4, b_5) = \oint_C (z^2, x^2) m_0 \, \mathrm{d}s$$

$$b_{14} = \oint_C m_2 \left(\frac{\mathrm{d}x}{\mathrm{d}s} \right)^2 \mathrm{d}s, \qquad b_{15} = \oint_C m_2 \left(\frac{\mathrm{d}z}{\mathrm{d}s} \right)^2 \mathrm{d}s$$

$$(b_{10}, b_{18}) = \oint_C \left[m_0 F_w^2(s), m_2 a^2(s) \right] \mathrm{d}s$$

in which

$$(m_0, m_2) = \sum_{k=1}^{m_l} \int_{h_{(k^-)}}^{h_{(k^+)}} \rho_{(k)} (1, n^2) \, \mathrm{d}n$$

where $h_{(k^+)} - h_{(k^-)}$ is the thickness of the kth layer and $\rho_{(k)}$ is the mass density of the kth layer.

The stress resultants N_{yy}, N_{sy} and stress couples L_{yy}, L_{sy} are defined as

$$(N_{yy}, N_{sy}, L_{yy}, L_{sy}) \equiv \sum_{k=1}^{m_l} \int_{h_{(k)}} (\sigma_{ss}, \sigma_{sy}, \sigma_{yy} n, \sigma_{sy} n) \, \mathrm{d}n$$

Appendix B: Definitions of Matrices in Eqs. (27) and (28) and of Nondimensional Parameters

Matrices in Eqs. (27) and (28) are defined as

$$[\boldsymbol{A}] = \begin{bmatrix} \boldsymbol{A}_s & \boldsymbol{B}_s \\ \boldsymbol{B}_d \boldsymbol{A}_s & \boldsymbol{A}_a + \boldsymbol{B}_a \boldsymbol{B}_s \end{bmatrix}, \qquad [\boldsymbol{A}_s]_{2m \times 2m} = \begin{bmatrix} \boldsymbol{0}_{m \times m} & \boldsymbol{I}_{m \times m} \\ -\bar{\boldsymbol{M}}_n^{-1} \bar{\boldsymbol{K}}_n & -\bar{\boldsymbol{M}}_n^{-1} \bar{\boldsymbol{C}}_n \end{bmatrix}, \qquad [\boldsymbol{B}_s]_{2m \times 4lm} = \begin{bmatrix} \boldsymbol{0}_{m \times 4lm} \\ \frac{1}{8\mu_0} \bar{\boldsymbol{M}}_n^{-1} \left[-A_1^c \boldsymbol{I}_{m \times m} \cdots A_l^{\mathrm{cMq}} \boldsymbol{I}_{m \times m} \right]_{m \times 4lm} \end{bmatrix}$$

$$\bar{\boldsymbol{M}}_n = \boldsymbol{\Theta}^T \bar{\boldsymbol{M}}_s \boldsymbol{\Theta}, \qquad \bar{\boldsymbol{C}}_n = \frac{1}{8\mu_0} \boldsymbol{\Theta}^T \bar{\boldsymbol{C}}_{\mathrm{ae}} \boldsymbol{\Theta}, \qquad \bar{\boldsymbol{K}}_n = \boldsymbol{\Theta}^T \left[k_r \bar{\boldsymbol{K}}_s + \frac{1}{8\mu_0} \bar{\boldsymbol{K}}_{\mathrm{ae}} \right] \boldsymbol{\Theta}, \qquad [\boldsymbol{A}_a]_{4lm \times 4lm} = \begin{bmatrix} -\beta_1^c \boldsymbol{I}_{m \times m} & & \\ & \ddots & \\ & & -\beta_l^{\mathrm{cMq}} \boldsymbol{I}_{m \times m} \end{bmatrix}$$

$$[\boldsymbol{B}_a]_{4lm \times 2m} = \begin{bmatrix} \begin{bmatrix} \boldsymbol{I}_{m \times m} \\ \vdots \\ \boldsymbol{I}_{m \times m} \end{bmatrix}_{lm \times m} \left[\boldsymbol{D}\boldsymbol{R}_1^c \quad \boldsymbol{D}\boldsymbol{R}_2^c \right]_{m \times 2m} \\ \begin{bmatrix} \boldsymbol{I}_{m \times m} \\ \vdots \\ \boldsymbol{I}_{m \times m} \end{bmatrix}_{lm \times m} \left[\boldsymbol{D}\boldsymbol{R}_1^{\mathrm{cq}} \quad \boldsymbol{D}\boldsymbol{R}_2^{\mathrm{cq}} \right]_{m \times 2m} \\ \begin{bmatrix} \boldsymbol{I}_{m \times m} \\ \vdots \\ \boldsymbol{I}_{m \times m} \end{bmatrix}_{lm \times m} \left[\boldsymbol{D}\boldsymbol{R}_1^{\mathrm{cM}} \quad \boldsymbol{D}\boldsymbol{R}_2^{\mathrm{cM}} \right]_{m \times 2m} \\ \begin{bmatrix} \boldsymbol{I}_{m \times m} \\ \vdots \\ \boldsymbol{I}_{m \times m} \end{bmatrix}_{lm \times m} \left[\boldsymbol{D}\boldsymbol{R}_1^{\mathrm{cMq}} \quad \boldsymbol{D}\boldsymbol{R}_2^{\mathrm{cMq}} \right]_{m \times 2m} \end{bmatrix}, \qquad \boldsymbol{D}\boldsymbol{R}_1^c = \boldsymbol{\Theta}_w^T \left[\frac{4 \tan \Lambda_e}{\mathcal{R}} \int_0^1 \hat{\boldsymbol{\Psi}}_w \hat{\boldsymbol{\Psi}}_w^T \, \mathrm{d}\eta \Theta_w - 2 \int_0^1 \hat{\boldsymbol{\Psi}}_w \hat{\boldsymbol{\Psi}}_\phi^T \, \mathrm{d}\eta \Theta_\phi \right]$$

$$
\boldsymbol{DR}_2^{c} = 4\Theta_w^T \int_0^1 \hat{\boldsymbol{\Psi}}_w \hat{\boldsymbol{\Psi}}_w^T \,\mathrm{d}\eta \boldsymbol{\Theta}_w, \qquad \boldsymbol{DR}_1^{\mathrm{cq}} = \boldsymbol{\Theta}_w^T \left[\frac{4\tan\Lambda_e}{\text{AR}} \int_0^1 \hat{\boldsymbol{\Psi}}_w \hat{\boldsymbol{\Psi}}_\phi^{\prime T} \,\mathrm{d}\eta \boldsymbol{\Theta}_\phi \right], \qquad \boldsymbol{DR}_2^{\mathrm{cq}} = 4\boldsymbol{\Theta}_w^T \int_0^1 \hat{\boldsymbol{\Psi}}_w \hat{\boldsymbol{\Psi}}_\phi^T \,\mathrm{d}\eta \boldsymbol{\Theta}_\phi
$$

$$
\boldsymbol{DS}_1^{\mathrm{cM}} = \boldsymbol{\Theta}_\phi^T \left[\frac{4\tan\Lambda_e}{\text{AR}} \int_0^1 \hat{\boldsymbol{\Psi}}_\phi \hat{\boldsymbol{\Psi}}_\phi^{\prime T} \,\mathrm{d}\eta \boldsymbol{\Theta}_w - 2\int_0^1 \hat{\boldsymbol{\Psi}}_\phi \hat{\boldsymbol{\Psi}}_\phi^T \,\mathrm{d}\eta \boldsymbol{\Theta}_\phi \right], \qquad \boldsymbol{DS}_2^{\mathrm{cM}} = 4\boldsymbol{\Theta}_\phi^T \int_0^1 \hat{\boldsymbol{\Psi}}_\phi \hat{\boldsymbol{\Psi}}_w^T \,\mathrm{d}\eta \boldsymbol{\Theta}_w
$$

$$
\boldsymbol{DS}_1^{\mathrm{cMq}} = \boldsymbol{\Theta}_\phi^T \left[\frac{4\tan\Lambda_e}{\text{AR}} \int_0^1 \hat{\boldsymbol{\Psi}}_\phi \hat{\boldsymbol{\Psi}}_\phi^{\prime T} \,\mathrm{d}\eta \boldsymbol{\Theta}_\phi \right], \qquad \boldsymbol{DR}_2^{\mathrm{cMq}} = 4\boldsymbol{\Theta}_\phi^T \int_0^1 \hat{\boldsymbol{\Psi}}_\phi \hat{\boldsymbol{\Psi}}_\phi^T \,\mathrm{d}\eta \boldsymbol{\Theta}_\phi
$$

$$
\bar{\boldsymbol{M}}_s = \int_0^1 \begin{bmatrix} \hat{\boldsymbol{\Psi}}_w \hat{\boldsymbol{\Psi}}_w^T & \boldsymbol{0} & \boldsymbol{0} \\ \boldsymbol{0} & \hat{I}_t \hat{\boldsymbol{\Psi}}_\phi \hat{\boldsymbol{\Psi}}_\phi^T + \hat{I}_w \hat{\boldsymbol{\Psi}}_\phi^{\prime} \hat{\boldsymbol{\Psi}}_\phi^{\prime T} & \boldsymbol{0} \\ \boldsymbol{0} & \boldsymbol{0} & \hat{r}^2 \hat{\boldsymbol{\Psi}}_x \hat{\boldsymbol{\Psi}}_x^T \end{bmatrix} \mathrm{d}\eta
$$

$$
\bar{\boldsymbol{K}}_s = \int_0^1 \begin{bmatrix} \frac{4}{\text{AR}^2} \hat{\boldsymbol{\Psi}}_w^{\prime} \hat{\boldsymbol{\Psi}}_w^{\prime T} & \frac{2}{\text{AR}} \mu_1 c_{14} \underline{\underline{\hat{\boldsymbol{\Psi}}_w^{\prime} \hat{\boldsymbol{\Psi}}_\phi^{\prime\prime T}}} & \frac{2}{\text{AR}} \hat{\boldsymbol{\Psi}}_w^{\prime} \Psi_x^T \\ & \frac{4}{\text{AR}^2} \mu_1 \mu_2 \underline{\underline{\hat{\boldsymbol{\Psi}}_\phi^{\prime\prime} \hat{\boldsymbol{\Psi}}_\phi^{\prime\prime T}}} + \mu_1 c_{12} \hat{\boldsymbol{\Psi}}_\phi^{\prime} \hat{\boldsymbol{\Psi}}_\phi^{\prime T} & \mu_1 c_{14} \underline{\underline{\hat{\boldsymbol{\Psi}}_\phi^{\prime\prime} \hat{\boldsymbol{\Psi}}_x^T}} + \mu_1 c_{13} \hat{\boldsymbol{\Psi}}_\phi^{\prime} \hat{\boldsymbol{\Psi}}_x^{\prime T} \\ \textbf{symm} & & \left(\mu_1 \hat{\boldsymbol{\Psi}}_x^{\prime} \hat{\boldsymbol{\Psi}}_x^{\prime T} + \hat{\boldsymbol{\Psi}}_x \hat{\boldsymbol{\Psi}}_x^T \right) \end{bmatrix} \mathrm{d}\eta
$$

In the preceding expressions $\hat{\boldsymbol{\Psi}}_w(\eta)$, $\hat{\boldsymbol{\Psi}}_\phi(\eta)$, and $\hat{\boldsymbol{\Psi}}_x(\eta)$ are shape function vectors (with dimension N) that are required to only fulfill the geometric boundary conditions. For the model incorporating both the warping restraint and transverse shear (WR + TS model), $\hat{\boldsymbol{\Psi}}_w(\eta) = [\eta, \eta^2, \ldots, \eta^N]^T$, $\hat{\boldsymbol{\Psi}}_\phi(\eta) = [\eta^2, \eta^3, \ldots, \eta^{N+1}]^T$, $\hat{\boldsymbol{\Psi}}_x(\eta) = [\eta, \eta^2, \ldots, \eta^N]^T$ are adopted in this paper. $\boldsymbol{\Theta}_w$, $\boldsymbol{\Theta}_\phi$, $\boldsymbol{\Theta}_x$ are $N \times m$ eigenvectors, and $\boldsymbol{\Theta} \equiv [\boldsymbol{\Theta}_w^T \ \boldsymbol{\Theta}_\phi^T \ \boldsymbol{\Theta}_x^T]^T$.

Nondimensional parameters used in the preceding equations are

$$
\mu_0 = \frac{b_1}{\pi \rho_\infty (2b)^2}, \qquad \mu_1 = \frac{a_{33}}{a_{55} L^2}, \qquad \mu_2 = \frac{a_{66}}{a_{33}(2b)^2}
$$

$$
\hat{r} = \sqrt{\frac{(b_4 + b_{14})}{b_1 L^2}}, \qquad c_{12} = \frac{a_{77}}{a_{33}}, \qquad c_{13} = \frac{a_{37}}{a_{33}}, \qquad c_{14} = \frac{a_{56}}{a_{33}}
$$

$$
\hat{I}_t = \frac{(b_4 + b_5)}{(2b)^2 b_1}, \qquad \hat{I}_w = \frac{(b_{10} + b_{18})}{L^2 (2b)^2 b_1}, \qquad k_r = \frac{a_{55}}{4 b_1 U_n^2}
$$

Matrix $\bar{\bar{\boldsymbol{K}}}_{\mathrm{ae}}$ in Eq. (29) is defined as

$$
\bar{\bar{\boldsymbol{K}}}_{\mathrm{ae}} = \int_0^1 \begin{bmatrix} \frac{2}{\pi} \frac{\tan\Lambda_e}{\text{AR}} \hat{\boldsymbol{\Psi}}_w \hat{\boldsymbol{\Psi}}_w^{\prime T} & -\frac{1}{\pi} \hat{\boldsymbol{\Psi}}_w \hat{\boldsymbol{\Psi}}_\phi^{\prime T} - \frac{\tan\Lambda_e}{\pi \text{AR}} \hat{\boldsymbol{\Psi}}_w \hat{\boldsymbol{\Psi}}_\phi^{\prime T} & \boldsymbol{0} \\ -\frac{\tan\Lambda_e}{\pi \text{AR}} \hat{\boldsymbol{\Psi}}_\phi \hat{\boldsymbol{\Psi}}_w^{\prime T} & \frac{1}{2\pi} \hat{\boldsymbol{\Psi}}_\phi \hat{\boldsymbol{\Psi}}_\phi^T + \frac{2}{3\pi} \frac{\tan\Lambda_e}{\text{AR}} \hat{\boldsymbol{\Psi}}_\phi \hat{\boldsymbol{\Psi}}_\phi^{\prime T} & \boldsymbol{0} \\ \boldsymbol{0} & \boldsymbol{0} & \boldsymbol{0} \end{bmatrix} \mathrm{d}\eta
$$

Acknowledgments

The authors gratefully acknowledge the very constructive comments from the anonymous referees and the Associate Editor.

References

[1]Shirk, M. H., Hertz, T. J., and Weisshaar, T. A., "Aeroelastic Tailoring–Theory, Practice and Promise," *Journal of Aircraft*, Vol. 23, No. 1, 1986, pp. 6–18.

[2]Librescu, L., and Song, O., "On the Static Aeroelastic Tailoring of Composite Aircraft Swept Wings Modeled as Thin-Walled Beam Structures," *Composites Engineering*, Vol. 2, No. 5–7, 1992, pp. 497–512.

[3]Jung, S. N., Nagaraj, V. T., and Chopra, I., "Assessment of Composite Rotor Blade Modeling Techniques," *Journal of the American Helicopter Society*, Vol. 44, No. 3, 1999, pp. 188–205.

[4]Song, O., "Modeling and Response Analysis of Thin-Walled Beam Structures Constructed of Advanced Composite Materials," Ph.D. Dissertation, Dept. of Engineering Science and Mechanics, Virginia Polytechnic Inst. and State Univ., Blacksburg, VA, Nov. 1990.

[5]Smith, E. C., and Chopra, I., "Formulation and Evaluation of an Analytical Model for Composite Box-Beams," *Journal of American Helicopter Society*, Vol. 36, No. 3, 1991, pp. 23–35.

[6]Rehfield, L. W., "Design Analysis Methodology for Composite Rotor Blades," *7th DoD/NASA Conference on Fibrous Composites in Structural Design*, AFWAL-TR-85-3094, June 1985, pp. (v(A)-1)–(v(A)-15).

[7]Librescu, L., and Song, O., "Behavior of Thin-Walled Beams Made of Advanced Composite Materials and Incorporating Non-Classical Effects," *Applied Mechanics Reviews*, Vol. 44, No. 11, Pt. 2, 1991, pp. S174–S180.

[8]Song, O., and Librescu, L., "Free Vibration of Anisotropic Composite Thin-Walled Beams of Closed Cross-Section Contour," *Journal of Sound and Vibration*, Vol. 167, No. 1, 1993, pp. 129–147.

[9]Na, S. S., "Control of Dynamic Response of Thin-Walled Composite Beams Using Structural Tailoring and Piezoelectric Actuation," Ph.D. Dissertation, Dept. of Engineering Science and Mechanics, Virginia Polytechnic Inst. and State Univ., Blacksburg, VA, Sept. 1997.

[10]Kim, C., and White, S. R., "Thick-Walled Composite Beam Theory Including 3-D Elastic Effects and Torsional Warping," *International Journal of Solids and Structures*, Vol. 34, No. 31–32, 1997, pp. 4237–4259.

[11]Bhaskar, K., and Librescu, L., "A Geometrically Non-Linear Theory for Laminated Anisotropic Thin-Walled Beams," *International Journal of Engineering Science*, Vol. 33, No. 9, 1995, pp. 1331–1344.

[12]Suresh, J. K., and Nagaraj, V. T., "Higher-Order Shear Deformation Theory for Thin-Walled Composite Beams," *Journal of Aircraft*, Vol. 33, No. 5, 1996, pp. 978–986.

[13]Wu, X. X., and Sun, C. T., "Vibration Analysis of Laminated Composite Thin-Walled Beams Using Finite Elements," *AIAA Journal*, Vol. 29, No. 5, 1991, pp. 736–742.

[14]Berdichevski, V. L., Armanios, E., and Badir, A., "Theory of Anisotropic Thin-Walled Closed Cross-Section Beams," *Composite Engineering*, Vol. 2, No. 5–7, 1992, pp. 411–432.

[15]Chandra, R., and Chopra, I., "Structural Response of Composite Beams and Blades with Elastic Couplings," *Composites Engineering*, Vol. 2, No. 5–7, 1992, pp. 347–374.

[16]Karpouzion, G., and Librescu, L., "Nonclassical Effects on Divergence and Flutter of Anisotropic Swept Aircraft Wings," *AIAA Journal*, Vol. 34, No. 4, 1996, pp. 786–794.

[17]Qin, Z., and Librescu, L., "On a Shear-Deformable Theory of Anisotropic Thin-Walled Beams: Further Contribution and Validation," *Journal of Composite Structures*, Vol. 56, No. 4, 2002, pp. 345–358.

[18]Bisplinghoff, R. L., Ashley, H., and Halfman, R. L., *Aeroelasticity*, Dover, New York, 1996.

[19]Singh, R., and Baeder, J. D., "Direct Calculation of Three-Dimensional Indicial Lift Response Using Computational Fluid Dynamics," *Journal of Aircraft*, Vol. 34, No. 4, 1997, pp. 465–471.

[20]Leishman, J., "Indicial Lift Approximations for Two-Dimensional Subsonic Flow as Obtained from Oscillatory Measurements," *Journal of Aircraft*, Vol. 30, No. 3, 1993, pp. 340–351.

[21]Marzocca, P., Librescu, L., and Chiocchia, G., "Aeroelastic Response of a 2-D Airfoil in a Compressible Flow Field and Exposed to Blast Loading," *Aerospace Science and Technology*, Vol. 6, No. 4, 2002, pp. 259–272.

[22]Leishman, J. G., "Validation of Approximate Indicial Aerodynamic Functions for Two-Dimensional Subsonic Flow," *Journal of Aircraft*, Vol. 25, No. 10, 1988, pp. 914–922.

[23]Silva, W. A., "Application of Nonlinear Systems Theory to Transonic Unsteady Aerodynamic Responses," *Journal of Aircraft*, Vol. 30, No. 5, 1993, pp. 660–668.

[24]Silva, W. A., "Dicrete-Time Linear and Nonlinear Aerodynamic Impulse Responses for Efficient (CFD) Analysis," Ph.D. Dissertation, Dept. of Applied Science, College of William and Mary, Williamsburg, VA, 1997.

[25]Qin, Z., Marzocca, P., and Librescu, L., "Aeroelastic Instability and Response of Advanced Aircraft Wings at Subsonic Flight Speeds," *Aerospace Science and Technology*, Vol. 6, No. 3, 2002, pp. 195–208.

[26]Marzocca, P., Librescu, L., and Chiocchia, G., "Aeroelastic Response of 2-D Lifting Surfaces to Gust and Arbitrary Explosive Loading Signatures," *International Journal of Impact Engineering*, Vol. 25, No. 1, 2001, pp. 41–65.

[27]Librescu, L., and Na, S. S., "Dynamic Response of Cantilevered Thin-Walled Beams to Blast and Sonic-Boom Loadings," *Shock and Vibration*, No. 5, 1998, pp. 23–33.

[28]Meirovitch, L., *Principles and Techniques of Vibrations*, Prentice–Hall, Upper Saddle River, NJ, 1997, pp. 189–194, 206–210.

[29]Librescu, L., Meirovitch, L., and Song, O., "Refined Structural Modeling for Enhancing Vibrations and Aeroelastic Characteristics of Composite Aircraft Wings," *La Recherche Aérospatiale*, No. 1, 1996, pp. 23–35.

[30]Qin, Z., "Vibration and Aeroelasticity of Advanced Aircraft Wings Modeled as Thin-Walled Beams," Ph.D. Dissertation, Dept. of Engineering Science and Mechanics, Virginia Polytechnic Inst. and State Univ., Blacksburg, VA, Oct. 2001.

[31]Librescu, L., Meirovitch, L., and Na, S. S., "Control of Cantilevers Vibration via Structural Tailoring and Adaptive Materials," *AIAA Journal*, Vol. 35, No. 8, 1997, pp. 1309–1315.

[32]Palazotto, A. N., and Linnemann, P. E., "Vibration and Buckling Characteristics of Composite Cylindrical Panels Incorporating the Effects of a Higher Order Shear Theory," *International Journal of Solids and Structures*, Vol. 28, No. 3, 1991, pp. 341–361.

[33]Goland, M., and Luke, Y., "The Flutter of a Uniform Cantilever Wing with Tip Weights," *Journal of Applied Mechanics*, Vol. 15, No. 1, 1948, pp. 13–20.

[34]Nelson, H. C., Rainey, R. A., and Watkins, C. E., "Lift and Moment Coefficients Expanded to the Seventh Power of Frequency for Oscillating Rectangular Wings in Supersonic Flow and Applied to a Specific Flutter Problem," NACA TN–3076, April 1954.

[35]Librescu, L., and Thangjitham, S., "Analytical Studies on Static Aeroelastic Behavior of Forward-Swept Composite Wing Structures," *Journal of Aircraft*, Vol. 28, No. 2, 1991, pp. 151–157.

[36]Weisshaar, T. A., "Forward Swept Wing Static Aeroelasticity," U.S. Air Force Wright Aeronautical Lab., Final Rept. AFWAL-TR80-3137, Wright–Patterson AFB, OH, Nov. 1980.

P. Weinacht
Associate Editor